Research Square

Preprints are preliminary reports that have not undergone peer review.
They should not be considered conclusive, used to inform clinical practice,
or referenced by the media as validated information.

SPARC is involved in the transition from DCIS to Invasive Ductal Carcinoma via a TGFBR- Dependent Mechanism in breast cancer

Marianela Sciacca
Universidad de Buenos Aires, Instituto de Oncología Ángel H. Roffo
Naira Rodríguez Padilla
Universidad de Buenos Aires, Instituto de Oncología Ángel H. Roffo
María del Pilar Carballo
Universidad de Buenos Aires, Instituto de Oncología Ángel H. Roffo
Ezequiel Lacunza
Universidad Nacional de La Plata
Paola de Luca
Universidad de Buenos Aires, Instituto de Oncología Ángel H. Roffo
Lina Marino
Universidad de Buenos Aires, Instituto de Oncología Ángel H. Roffo
Paola Noelia Cardozo
Universidad de Buenos Aires
Tamara López-López
University Medical Center Hamburg-Eppendorf
Martin Abba
Universidad Nacional de La Plata
Laura Courtois
Institut Curie
Ivan Bieche
Institut Curie
Anne Vincent-Salomon
Institut Curie
Érica Rojas Bilbao
Universidad de Buenos Aires, Instituto de Oncología Ángel H. Roffo
Katrina Podsypanina
Institut Curie, CNRS UMR 144, PSL University
Mathieu Boissan
Sorbonne Université, INSERM, Centre de Recherche Saint-Antoine
Philippe Chavrier

Institut Curie, CNRS UMR 144, PSL University

Ana María Eiján

Universidad de Buenos Aires, Instituto de Oncología Ángel H. Roffo

Pablo J Sáez

University Medical Center Hamburg-Eppendorf

Catalina Lodillinsky

clodillinsky@cbc.uba.ar

Universidad de Buenos Aires, Instituto de Oncología Ángel H. Roffo

---

Research Article

Keywords: Ductal carcinoma in situ, SPARC, Breast cancer, TGF-B

Posted Date: June 19th, 2026

DOI: https://doi.org/10.21203/rs.3.rs-9752553/v1

License: This work is licensed under a Creative Commons Attribution 4.0 International License.
Read Full License

Additional Declarations: No competing interests reported.

Abstract

Background

Ductal carcinoma in situ (DCIS) is a pre-invasive lesion with variable risk of progression to invasive ductal carcinoma (IDC), however, reliable predictors of invasive transition remain lacking. Membrane type I matrix metalloproteinase (MT1-MMP) is a key regulator of DCIS progression.

Methods

We combined RNA sequencing of MT1-MMP^{high} and MT1-MMP^{low} cell populations from intraductal tumor xenografts with human high-grade DCIS datasets to identify regulators of early breast cancer progression.

Results

Secreted Protein Acidic and Cysteine Rich (SPARC) was identified as a candidate associated with the invasive switch. SPARC was upregulated in DCIS compared to normal breast epithelium and increased in IDC, and correlated with MT1-MMP expression. Functionally, SPARC depletion reduced MT1-MMP expression, matrix degradation, and TGF-β signaling activity, while TGF-β receptor type I (TGFBRI) inhibition decreased SPARC and MT1-MMP levels, matrix degradation and cell migration. In a new triple-negative intraductal syngeneic mouse model, TGFBRI inhibition reduced the transition from in situ to invasive lesions and decreased SPARC and MT1-MMP expression. Notably, SPARC expression was not associated with metastatic dissemination, supporting a role in early progression.

Conclusions

Our findings identify SPARC as a TGF-β–dependent regulator of early breast cancer progression and highlight the TGFBRI–SPARC–MT1-MMP axis as a potential therapeutic target.

Background

Female breast cancer is the most commonly diagnosed cancer worldwide, with approximately 2.3 million new cases and more than 0.65 million deaths annually[1]. The consequences of this disease highlight the need for new molecular targets to predict recurrence and/or progression and improve existing therapies.

Breast carcinomas are classified based on the presence or absence of invasion into ductal carcinoma in situ (DCIS) and invasive ductal carcinoma (IDC). DCIS is defined as a proliferation of neoplastic epithelial cells confined within the mammary ductal system and separated from the surrounding stroma by an

intact basement membrane and myoepithelial layer[2]. Although most DCIS lesions are asymptomatic, their incidence has increased markedly with the widespread use of mammographic screening and now accounts for up to 30% of newly diagnosed breast cancers[3]. DCIS comprises a heterogeneous group of lesions with diverse histological, molecular, and clinical features[4–6]. While it is widely considered a non-obligate precursor of IDC, the factors that determine progression to invasive disease remain largely unknown. As a result, current management strategies may lead to overtreatment of indolent lesions or undertreatment of aggressive ones. This challenge is particularly evident in patients with hormone receptor–negative tumors, for whom targeted therapeutic options remain limited[7].

Extracellular matrix remodeling is a critical step in tumor invasion. MT1-MMP is highly expressed at the invasive front of breast carcinomas and plays a central role in matrix degradation and tumor cell invasion. We previously demonstrated that MT1-MMP is required for the transition from DCIS to IDC in the intraductal xenograft mouse model[8].

In the present study, we sought to identify additional molecular regulators associated with MT1-MMP–driven breast cancer progression. By integrating transcriptomic profiling of MT1-MMP^{high} tumor cell populations with human high-grade DCIS datasets, we identified SPARC as a candidate mediator of the invasive switch. We show that SPARC expression correlates with MT1-MMP in patient samples and is dynamically upregulated during early breast cancer progression. Furthermore, it functionally regulates MT1-MMP expression, matrix degradation, and tumor invasion, and is involved in a TGF-β–dependent regulatory network.

Using both *in vitro* systems and a new triple negative intraductal syngeneic mouse model, we further demonstrate that pharmacological inhibition of TGF-β signaling restrains invasive progression by targeting the SPARC–MT1-MMP axis. Thus, we propose that blockade of the TGFBRI/SPARC/MT1-MMP axis, may offer therapeutic improvements to patients with SPARC-positive in situ tumors.

Methods

Cell Culture

MCF10DCIS.com (MCF10DCIS herein) cell line (CVCL_5552) was purchased from Asterand (Detroit, MI, USA) and maintained in advanced DMEM/F12 media supplemented with 10% fetal bovine serum (FBS) and 2 mM glutamine at 37°C in 5% CO_2. Murine breast cancer cell line LM38-LP (CVCL_B7PY)[9] was maintained in DMEM-F12 medium (Gibco) supplemented with 2 mM L-glutamine, 80 µg/ml gentamycin and 10% FBS (Internegocios, Argentina) in a humidified atmosphere with 5% CO_2 at 37°C. Serial passages of confluent monolayers were performed by detaching cells with trypsin (0.25% trypsin and 0.075% EDTA in Ca^{2+} and Mg^{2+} free PBS). All experiments were performed with mycoplasma-free cells and the human cell line, MCF10DCIS has been authenticated using STR profiling.

Cell Isolation, transcriptomic analysis and Target Gene Selection

Invasive tumors generated after intraductal injection of MCF10DCIS cells in the mammary gland of SCID mice[8] were harvested and mechanically dissociated. FACS based on human CD298 (BD Pharmingen™, clone LNH-94) and MT1-MMP (Millipore Anti-MMP-14, catalytic domain, clone LEM-2/15.8) antibodies was performed. Based on MT1-MMP expression levels, two different cell populations defined as MT1-MMP^{high} and MT1-MMP^{low} were obtained. After RNA purification, samples were processed according to the protocol of SMARTer stranded total RNA seq Kit-Pico Input Mammalian, and then sequenced using HISeqTM, of Illumina at the *Core Facility* of the Institut Curie, Paris, France.

Briefly, FASTQ files generated from sequencing each sample were used to align the sequencing reads to the human genome, producing BAM files. To perform this alignment, we employed the SubRead package within the R/Bioconductor environment. Following alignment, we used Trimmomatic to trim the reads, ensuring data quality and accuracy. The BAM files, after alignment and trimming, were then processed to create a read counts matrix. This matrix served as the input for DESeq2, another R/Bioconductor package, which was utilized to identify differentially expressed genes between the two study groups. The entire analysis was conducted within the R statistical environment

To identify similarities in gene expression between our experimental model and human high-grade DCIS samples, we compared the list of genes upregulated in the MT1-MMP^{high} population of our model with those identified in the human DCIS-C1 and DCIS-C2 subsets. As described by Abba et al. (2015)[10], these two DCIS subgroups were defined based on their tumor-intrinsic subtypes, proliferative and immune scores, and activity of specific signaling pathways. The more aggressive DCIS-C1 subgroup, which is highly proliferative and basal-like or ERBB2(+), exhibited signatures of activated regulatory T cells and immunosuppressive complexes, reflecting a tumor-associated immune suppression, indicative of a tumor-associated immunosuppressive phenotype. This classification provided a valuable framework for comparing the gene expression profiles of our experimental model with those of human DCIS.

Human Tissue samples

Formalin-Fixed Paraffin-Embedded (FFPE) human breast tumor tissue were collected from three different cohort of patients. PIC-BIM cohort: 116 primary breast tumor samples were collected at Institut Curie from 2005 to 2006 prior to any radiation, hormonal or chemotherapy treatment. Roffo cohort I: 58 primary breast tumors were collected from 2015 to 2016 and Roffo cohort II: 57 samples of primary breast tumors harbouring IDC and lymph node metastasis were collected from 2015 to 2020 at Instituto de Oncología A. H. Roffo (SI Table S1).

All women provided a signed informed consent for future biomarker research studies. Data were analyzed anonymously. This study complies with the Declaration of Helsinki, and was approved by each institution's internal review and ethics board (Comité de Pilotage du Groupe Sein, Institut Curie). Immunohistochemical (IHC) analysis of human samples was performed following approval by the

institutional review board of the Comité de Ética en Investigación Clínica–Instituto Ángel H. Roffo (21/18).

Tumor breast molecular subtypes were defined as follows according to the guidelines of the American Society of Clinical Oncology (ASCO)/College of American Pathologists[11,12]. Luminal A: estrogen-receptor (ER) ≥ 10%, progesterone-receptor (PR) ≥ 20%, Ki-67 < 14%; Luminal B: ER ≥ 10%, PR < 20%, Ki-67 ≥ 14%; HER2+: ER < 10%, PR < 10%, HER2 2 + amplified or 3+; Triple negative breast cancers (TNBC): ER < 10%, PR < 10%, HER2 0/1 + or 2 + non-amplified. Clinical and pathological features of patients are summarized in Table S1.

Metastasis-free survival (MFS) was determined as the interval between diagnosis and detection of the first metastasis. Survival distributions were estimated by the Kaplan-Meier method, and the significance of differences between survival rates was ascertained using a log-rank test. GraphPad Prism (GraphPad Software) was used for statistical analysis.

siRNA treatment, Cell viability assay and cell count assay

Small interfering RNA (siRNA) transfection was performed using 5 nM siRNA with Mission®siRNA Trasfection Reagent (Sigma) according to the manufacturer's instructions. The following siRNAs were used: esiRNA cDNA target sequence Human siSPARC: EHU002941, Mouse siSPARC: EMU088951; MISSION® siRNA Universal Negative Control #1: sic001 (Sigma). Subconfluent monolayers of tumoral cells (LM38-LP or MCF10DCIS) were transfected with SPARC siRNA according to the manufacturer's instructions. $3x10^3$ cells/100 µl were cultured in 96-well plates and cell viability was analyzed 72 h after transfection. RTq-PCR, IF and gelatin degradation assay were performed in parallel. For testing the involvement of the TGF-β pathway on cell viability, LM38-LP cell line was treated with TGF-β (2 ng/ml, Peprotech) or SB431542 (20 ng/ml, StemCell) for 48 h. Cell viability was determined by the Cristal violet assay (Promega).

Quantitative real time PCR

Total RNA from murine or human cell lines, were isolated with TRIZol Reagent (Invitrogen) as described[13]. Briefly, cDNA was synthesized using RT-PCR SuperScript™ III One-Step (Invitrogen) and used as template for qPCR analyzing using TransStart Green qPCR SuperMix (TransGen Biotech) and reactions were carried out in the CFX96 Real-Time System, C1000-Thermal-Cycler (Biorad). Specific primers details and RT-qPCR procedure are listed in supplementary information.

Western blot assay

Subconfluent monolayers of tumor cells (LM38-LP or MCF10DCIS) were transfected with SPARC siRNA or were treated with or without SB431542. Detailed procedure is listed in Supplementary information.

Immunofluorescence analysis

LM38-LP or MCF10DCIS cells grown in complete medium on chamber slides were transfected with SPARC siRNA. Detailed procedure is listed in Supplementary information.

Fluorescent Gelatin Degradation Assay

Assays of fluorescent gelatin degradation were performed and quantified as previously described[15]. Detailed procedure is listed in Supplementary information.

Migration assays

To monitor cell migration in complex 3D microenvironments we used collagen gels following an established method[16–18]. The device was fabricated by curing polydimethylsiloxane (PDMS) on a silicone mold with a positive relief of three compartments previously described[17]. The resultant PDMS channel was bonded to a glass bottom Petri dish (Fluorodish) at 65°C for 20 min. Then, rat tail type I collagen (Corning) was diluted to a final concentration of 2 mg/mL in PBS pH 8.0. The cells were added in medium with a final concentration of $6x10^5$ cells/ml. The gels polymerized after 20 min of incubation at 37°C. After the administration of the corresponding treatments cellular behavior was monitored using an inverted microscope (Leica Dmi8) equipped with an APO 10x/0.45 PH1, FL L 20x/0.40 CORR PH1, and APO 40x/0.95 objectives. Images were recorded with an ORCA-Flash4.0 Digital camera (Hamamatsu Photonics) using the MetaMorph Version 7.10.3.279 software (Molecular Device). Images were captured every 3 min for 16 h, employing 10x magnification with PH1 phase contrast and binning set to 2.

For 2D migration experiments, $1.5x10^3$ cells were plated on a glass bottom dish and treated for 2 h with TGF-β (2 ng/ml, Peprotech) or SB431542 (20 ng/ml, StemCell) and stained with Hoesch (Invitrogen). Cells were monitored using the same system described for 3D, using 10x magnification and for a total duration of 4.5 h. Cell tracking was performed by combining previously described methods[17,18]. Briefly, raw movies were processed, and later on tracked by using TrackMate v7 plugin from Fiji (ImageJ) to obtain the main migration parameters[17,18].

Intraductal tumor growth

Ten-week-old female BALB/c mice obtained from our Institute Animal Care Division were inoculated intraductally in the fourth pair of mammary glands with $5x10^3$ LM38-LP cells as previously described[8,19]. After three weeks mice were randomized into 2 groups: Control and Galunisertib (n = 10 per group). After the detection of any palpable tumor (around the third week) Galunisertib was orally administered once a day at a dose of 60mg/kg for 5 days. Then, mammary glands were harvested and processed for histological procedures. Mice were handled in accordance with the international procedure for Care and

Use of Laboratory Animals. Protocols were approved by the Institutional Review Board CICUAL, Institute of Oncology Angel H. Roffo (04/2023).

Histological and immunofluorescence analysis of mouse tissue sections

Whole-mount carmine staining and hematoxylin and eosin (H&E) staining of tissue sections were carried out as previously described[20]. After whole mount staining, image acquisition was performed with a Zeiss Stemi 2000-C Stereo Microscope. Quantification of the tumor area was performed using Image J software. To retrieve antigens on paraffin-embedded tissue samples, sections were incubated for 20 min in 10 mM sodium citrate buffer, pH 6.0 at 90°C. Then, after 60 min incubation in 5% FCS, sections were incubated overnight with diluted primary antibodies, washed and further incubated for 2 h at room temperature with appropriate secondary antibodies. Conventional Hematoxylin (Biopur) and Eosin (Merk) staining was carried out according to manufacturer's instructions.

Antibodies

Antibodies for immunofluorescence and IHC are detailed in Supplementary information.

Gene Expression Data Analysis

To examine the association and co-expression of genes in breast cancer tissues, data were extracted from cBioPortal for Cancer Genomics (https://www.cbioportal.org/), which provides visualization, analysis, and download of large-scale cancer genomics data sets[21] by specifically focusing on TCGA (The Cancer Genome Atlas) research network database. For assessing the expression of SPARC and MT1-MMP in breast cancer cell lines, we utilized RNA sequencing data from the GSE48213 dataset, which includes comprehensive transcriptional profiling of a breast cancer cell line panel. Additionally, timeline data documenting the progression from normal breast tissue to invasive breast cancer was generously provided by Rebbeck et al[22]. To define the network connectivity and functional associations between coexpressed genes, we utilized the STRING web tool (https://string-db.org/), which provides a comprehensive analysis of known and predicted protein-protein interactions. In addition, we employed the Gene Ontology (GO) analysis tools integrated within STRING to further investigate the biological processes, molecular functions, and cellular components associated with these genes, allowing for a deeper understanding of their potential roles in the studied context.

Statistical analysis

Data are expressed as the mean ± SD or ± SEM. Statistical analyses of H-score, protein and mRNA and protein levels, gelatin degradation assay, cell survival, migration and invasion assays were performed using X^2 test, Student's t-test, one-way or two-way analysis of variance using GraphPad Prism (GraphPad Software, La Jolla, CA, USA) as specified in each figure legend. A p value < 0.05 was considered statistically significant.. For survival analysis, Kaplan–Meier plots were drawn and statistical differences evaluated using the log-rank test. For correlation analysis in cell lines, andpatient samples Pearson's

correlation was used. For gene expression boxplots, the Wilcoxon rank-sum test was used.. (R software version 3.0.2, R Foundation for Statistical Computing, Institute for Statistics and Mathematics, Vienna, Austria).

Results

SPARC is a candidate regulator of early breast cancer progression

We previously showed that MT1-MMP expression is upregulated in invasive as compared to in situ breast carcinomas and correlates with poor clinical outcome[8]. In addition, we found that MT1-MMP expression is required for the DCIS-to-invasive transition of breast tumor xenografts formed upon intraductal injection of MCF10DCIS cells in the mammary gland of immunocompromised SCID mice[8]. Building on these findings, we sought to identify additional molecular determinants associated with MT1-MMP–driven breast cancer progression. To this end, we performed RNA sequencing of MT1-MMP^{high} and MT1-MMP^{low} tumor cell populations isolated from invasive breast tumors in the intraductal xenograft model.

Differential expression analysis identified 47 significantly deregulated genes, the vast majority of which were upregulated in MT1-MMP^{high} tumor cells (p value < 0.05, DR < 0.05). These genes were enriched in biological processes related to extracellular matrix organization and integrin-mediated adhesion (p < 0.01), consistent with the well-established role of MT1-MMP in matrix remodeling during tumor invasion (Fig. 1A and Supp file 1).

To assess the clinical relevance of this signature, we compared it with transcriptomic data from human high-grade DCIS subgroups classified as aggressive (DCIS-C1) or indolent (DCIS-C2) [10]. No overlap was observed with the indolent DCIS-C2 subgroup, whereas three genes – *SPARC*, Cyclooxygenase-2 (PTGS2), and Calcium-Activated Chloride Channel regulator 2 (CLCA2) – were shared between MT1-MMP^{high} tumor cells and the aggressive DCIS-C1 subgroup (Fig. 1B–C). These genes displayed similar expression changes in MT1-MMP^{high} *vs.* MT1-MMP^{low} tumor cells and in aggressive DCIS-C1 *vs.* indolent DCIS-C2 subgroups. Among these candidates, SPARC showed the strongest positive correlation with MT1-MMP expression in breast cancer datasets at both the mRNA and protein levels (Fig. 1D). Immunohistochemical (IHQ) analysis on xenograft tumor sections further revealed co-localization of SPARC and MT1-MMP at the invasive front of MCF10DCIS tumor xenografts (Fig. 1E). Taken together these findings identify SPARC as a candidate gene associated with MT1-MMP–driven he regulation of the invasive switch of breast cancer.

SPARC is dynamically upregulated during early breast cancer progression

We next examined SPARC expression in human breast tissue samples including normal breast, DCIS, and IDC components from two independent breast cancer patient cohorts (PIC-BIM, n = 78; Roffo, n = 34). In line with previous reports[23], SPARC signal was detected in myoepithelial cells of normal mammary ducts, in tumor-associated fibroblasts and in endothelial cells (data not shown). Overall, SPARC was undetectable in normal breast epithelium, upregulated in DCIS, and further increased in matched IDC across both cohorts (Fig. 2A-C). In addition, the proportion of SPARC-positive IDC tumors was higher in high-grade than in lower-grade breast cancers (Fig. 2D). When IDC tumors were stratified into breast molecular subtypes, SPARC expression was higher in TNBC (Fig. 2E).

Recently, it was proposed that the progression from in situ lesions to IDC involves dual, early and late epithelial-to-mesenchymal transition (EMT) events[22]. Pseudo-time analyses of matched DCIS and IDC samples have revealed a continuum of transcriptional states, in which DCIS lesions exhibit varying degrees of similarity to either normal epithelium or invasive carcinoma[22]. To determine whether SPARC follows this dynamic progression, we analyzed its expression along a pseudo-time trajectory derived from matched DCIS and IDC samples. SPARC displayed, similar to EMT genes, a biphasic expression pattern, with two distinct peaks reminiscent of EMT-associated states, suggesting that it may contribute to both early and intermediate stages of invasive progression (Fig. 2F, left panel). Consistent with immunohistochemistry (IHC) data, *SPARC* transcript levels were highest in IDC samples (Fig. 2F, right panel). We next examined the relationship between SPARC and MT1-MMP in breast cancer patient specimens. In the Roffo cohort, a significant fraction of DCIS lesions exhibited concomitantly high SPARC and MT1-MMP expression in carcinoma cells (Fig. 2G-I), in which MT1-MMP displayed membrane-associated or granular cytoplasmic localization. These findings indicate that SPARC and MT1-MMP are coordinately expressed in both experimental xenograft model (Fig. 1E) and human lesions.

To determine whether SPARC represents a general marker of tumor progression or is specifically associated with early invasive stages, we analyzed a third independent cohort including IDC and matched lymph node metastases. In contrast to primary lesions, metastatic tissues lacked SPARC expression in neoplastic cells (Figure supp 1A-C). Consistently, SPARC expression was not associated with metastasis-free survival (Figure supp 1D, supp 2B). These results suggest that SPARC is specifically involved in early invasive progression. SPARC expression is present in the healthy stroma[23]. In our cohorts, SPARC expression in the tumor stroma did not show significant differences with respect to the molecular subtypes (data not shown). Furthermore, expression of SPARC and MT1-MMP increased concomitantly in cell lines with basal features (Figure supp 2A), consistent with the idea that co-regulation of these genes may be informative only in the neoplastic compartment. To further deepen our analysis, the prognostic power of SPARC and MT1-MMP co-expression was evaluated by RTqPCR in a retrospective cohort of 458 breast cancer patients in which we previously reported that MT1-MMP up-regulation correlated with shorter metastasis-free survival (MFS) (Figure supp 2B, left panel and Ref [8]). However, neither SPARC nor combination of SPARC and MT1-MMP expression impacted metastasis-free

survival (Figure supp 2B, middle and right panel). These findings indicate that, unlike MT1-MMP, SPARC is restricted to early stages of tumor progression and acts in concert with MT1-MMP.

MT1-MMP mediates the invasive potential of SPARC

To strengthen our findings in an immunocompetent murine model, we analyzed the role of SPARC in early breast cancer progression using the mouse mammary cancer cell line LM38-LP [9], which was inoculated in the ductal system of syngeneic mice (Figure sup 3A). Whole-mount and histology staining revealed in situ tumors three weeks post-intraductal injection of LM38-LP cells. A continuous layer of elongated α-SMA positive myoepithelial cells segregating *in situ* tumors from the stroma was observed (Figure supp 3B). During the fifth week, LM38-LP tumors spontaneously progressed to invasive lesions characterized by disrupted stromal collagen organization (Figure supp 3AB). These tumors were negative for ER, PR and HER2/neu (Figure supp 3C). Thus, we concluded that LM38-LP xenograft tumors are an appropriate model to study the molecular events involved in the early transition of triple-negative breast cancer in immunocompetent mice. Both LM38-LP tumor cells in culture and derived tumors from the syngeneic intraductal mouse model expressed SPARC and MT1-MMP with a perinuclear granular distribution (Figure supp 4A). Knockdown of SPARC by RNAi did not affect cell proliferation or morphology (Figure supp 4B and C). In contrast, SPARC silencing reduced MT1-MMP expression in both human MCF10DCIS and murine LM38-LP tumor cells (Fig. 3A-C and supp 4D-E), resulting in decreased matrix degradation capacity (Fig. 3DE). Together, these results demonstrate that SPARC promotes tumor invasion through regulation of MT1-MMP.

SPARC and MT1-MMP are regulated within a TGF-β–dependent network

To profile molecules involved in the early transition, we used a subset of publicly available breast cancer data from the TCGA database to conduct a gene co-expression analysis of the three previously identified genes, *SPARC, PTGS2*, and *CLCA2* together with *MMP14* (encoding MT1-MMP), across five breast cancer subtypes: Luminal A (LumA, n = 473), Luminal B (LumB, n = 205), Her2 (n = 86), Normal-like (NL, n = 73), and Basal (n = 185) tumor subtypes and also in adjacent normal tissue (NAT, n = 103) (Supp file 1).

Analysis of co-expressed genes from each gene list ($R > 0.5$, $p < 0.0001$), irrespective of breast cancer molecular subtypes, revealed three common genes: MYLK, EGFR, and ADAMTS9 co-expressed with all the four candidate genes (Figure supp 5A). SPARC and MMP14 exhibited the highest number of partners (Figure supp 5B). Focusing on genes co-expressed with individual candidate genes across all breast cancer groups, we identified 161 genes for *SPARC*, 51 for *MMP14*, 10 for *PTGS2* (except in Basal), and none for CLCA2 (Supp file 1). Notably, only *SPARC* and *MMP14* shared common partners (Figure supp 5B): *COL6A2, AEBP1, COL5A1, MMP2, BMP1, COL1A2, COL6A1, COL1A2, PCOLCE, COL3A1, ST3GAL2, SYDE1, GPR124*. Further analysis of these 13 shared genes and the three genes coexpressed in all five breast cancer groups revealed a strong association among 80% of them. Integration of these genes

revealed a highly interconnected network enriched in collagen organization, matrix degradation, and TGF-β signaling pathways (Fig. 4A).

We experimentally confirmed the involvement of the TGF-β pathway in the SPARC-dependent cell survival, as treatment of LM38-LP cells with TGF-β increased cell viability, while treatment with TGFBRI inhibitor, SB431542, abolished the survival response (Fig. 4B). Although treatment of LM38-LP cells with TGF-β did not affect SPARC expression (data not shown). Inhibition of TGF-β signaling with SB431542 decreased both SPARC and MT1-MMP expression at the mRNA and protein levels, suggesting that activation of TGFBRI signaling contributes to steady-state SPARC and MT1-MMP expression in both LM38-LP and MCF10DCIS cell lines (Fig. 4C-F and supp 5CD). To test the involvement of SPARC in canonical activation of the TGF-β pathway, we evaluated the phosphorylation status of SMAD2/3 acting downstream of TGFBRI. In cells knocked down for SPARC, p-SMAD 2/3 levels were reduced (Fig. 4G), implying that SPARC is required for optimal activation of the TGF-β signaling pathway. Functionally, inhibition of TGFBRI using two different pharmacological inhibitors, SB431542 and Galunisertib, decreased matrix degradation (Fig. 5A-D). To determine the effect of TGF-β pathway modulation on motility, we monitored single cell migration in 3D collagen matrices[17], which mimic interstitial migration. TGF-β accelerated the mean speed of LM38-LP cells as compared to control, while treatment with SB431542 reduced cell motility in both LM38-LP and MCF10DCIS cell lines (Fig. 5E and Figure supp 5E). Interestingly, the effect of SB431542 treatment was lost in silencing of SPARC in LM38-LP cells, confirming that TGFBRI-induced cell motility is at least partially dependent on SPARC (Fig. 5F). Collectively, these findings identify a TGF-β–dependent regulatory axis in which SPARC controls MT1-MMP expression and tumor cell invasion.

Inhibition of TGF-β signaling pathway restrains invasive progression in a syngeneic intraductal mouse model

To validate the functional association between SPARC and the TGF-β pathway in vivo, we used the LM38-LP intraductal syngeneic mouse model (Figure supp 3A). SPARC and TGFBRI expression were enriched at the invasive tumor front (Figure supp 5F), supporting activation of this pathway during early breast cancer progression. Treatment of tumor-bearing mice with the TGFBRI inhibitor Galunisertib resulted in a marked reduction in invasive lesions, as assessed by whole-mount carmine staining and histological analysis (Fig. 6A-C). The invasive tumor area was also significantly decreased in treated mice (Fig. 6D). Moreover, Galunisertib-treated tumors contained fewer proliferating cells, as determined by Ki67 staining, and less nuclear SMAD-4, consistent with an effective blockade of TGFBRI signalling. Furthermore, tumors from Galunisertib-treated mice showed lower SPARC and MT1-MMP intensity as compared to untreated controls (Fig. 6E-F). Consistently, analysis of human breast cancer datasets further revealed that SPARC expression positively correlated with TGF-β and TGFBRI in breast cancer specimens at the mRNA levels (Fig. 6G). Together, these results demonstrate that pharmacological inhibition of TGFBRI limits the transition from in situ to invasive carcinoma, at least in part through suppression of the SPARC–MT1-MMP axis.

Discussion

Understanding the molecular mechanisms that trigger the formation of invasive tumors from *in situ* lesions is of paramount importance to select appropriate treatment strategies for women diagnosed with early breast cancer. In the absence of robust predictive biomarkers many patients may receive unnecessary treatment. Experimental models that faithfully recapitulate the DCIS-to-IDC transition in breast cancer progression provide a valuable framework to address this challenge.

We have previously reported an essential role of extracellular matrix-degradative and basement membrane-breaching MT1-MMP in DCIS-to-IDC transition using the human-in-mouse intraductal xenograft system of MCF10DCIS cells in immunodeficient mice[8,19,24]. Building on these findings, we sought to identify additional molecular regulators associated with MT1-MMP–driven breast cancer progression. Here, using computational analysis of gene signatures derived from MT1-MMP^{high} and MT1-MMP^{low} cells from intraductal MCF10DCIS cell tumor xenografts revealed a significant enrichment of genes involved in processes associated with cell adhesion and extracellular matrix remodelling[25]. Alignment of MT1-MMP^{high} cell and high-grade DCIS-C1 cohort[10] gene expression profiles identified three common genes. Up-regulation of these genes in the context of DCIS-to-IDC progression both in the experimental and clinical settings prompted us to investigate these molecules as possible players in the prelude to invasive transition. Among the three candidates, SPARC, was best correlated with MT1-MMP expression. SPARC has been described pro- or anti-tumor roles in different cancers[26]. In advanced breast cancer patients low levels of SPARC protein correlated with worse prognosis[27]. In contrast, in multivariate analysis, high SPARC expression was independently predictive for disease-free-survival in all patients[28,29]. Although SPARC has been reported to exert context-dependent pro- or anti-tumorigenic functions[29,30], our data support a pro-tumorigenic role during early breast cancer progression.

Although strong SPARC expression in the tumor stroma was associated with shorter time to recurrence among DCIS patients[23], in this study we centered our investigation on neoplastic epithelial cells. In this work, based on IHC analysis of FFPE tumor samples from three independent cohorts totaling 230 samples and including different stages of invasion, we found that SPARC expression was absent in normal breast epithelium, elevated in DCIS, and further increased in IDC, particularly in aggressive tumors. In contrast, SPARC was absent in lymph node metastases and did not correlate with patient outcome, indicating that its role is restricted to early invasive progression rather than late-stage dissemination. These findings distinguish SPARC from general prognostic markers and instead position it as a stage-specific regulator of local tumor invasion.

Recent gene expression analysis of over 2,000 individually microdissected ductal lesions revealed that the progressive loss of basement membrane integrity, which signifies transition towards invasive carcinoma, involves two distinct epithelial-to-mesenchymal transition (EMT) events. The initial EMT event occurs early in progression, while a second event happens later, coinciding with convergence of expression profiles between ductal carcinoma in situ (DCIS) and invasive ductal carcinoma (IDC)[22].

Overexpression of SPARC can promote cell migration and invasion and correlates with expression of mesenchymal markers in several types of cancer cells[31,32]. In addition, SPARC has been shown to increase expression or activation of a number of metalloproteinases in a fibroblastic and inflammatory context[33] and in some cancer cells[34,35]. Consistently, our data demonstrate that SPARC functionally controls MT1-MMP expression and matrix degradation in both human and mouse breast cancer models. These findings establish a direct mechanistic link between SPARC and the acquisition of invasive properties.

At the molecular level, our analyses revealed that SPARC and MT1-MMP are involved within a shared transcriptional network enriched in extracellular matrix components and TGF-β signaling pathway genes.

This finding is consistent with reports indicating that SPARC acts extracellularly as a mediator of TGF-β signalling in various contexts, including fibrosis and EMT promotion in lung cancer cells[36–38]. In this study, we extend these observations to breast cancer, showing that in tumour cells of human or mouse origin, blocking TGFBRI activity reduces SPARC and MT1-MMP expression. As a consequence, the invasive properties of tumor cells, such as matrix degradation and motility are decreased. We speculated that DCIS-to-IDC progression is driven by TGF-β-dependent increase in SPARC and MT1-MMP levels. Secreted SPARC may interact with TGFBRI in tumor microenvironment[39]. In vitro, treatment with SPARC did not increase p-SMAD levels in tumor cells (data not shown), suggesting that TGFBRI activation is maximal in cells in culture. On the other hand, KO SPARC cells down-modulate p-SMAD2/3. One possible scenario is that basal TGF-β activity induces SPARC expression as part of the first wave of EMT, while secreted SPARC amplifies TGFBRI signaling to induce MT1-MMP expression, participating in the second EMT wave and to DCIS-to-IDC transition. This leads us to hypothesize that basal levels of SPARC, when secreted, activates signaling molecular pathway trigged by the TGFBRI such as MT1-MMP expression, one of the target genes of this pathway.

LM38-LP, a triple negative mouse cell line of breast cancer, was positive for SPARC and MT1-MMP. In this work we described for the first time that this cellular model is able to develop *in situ* tumors after intraductal injection in syngeneic mice. These intraductal tumors spontaneously progress into invasive ones, which makes this model an excellent tool for studying molecular factors involved in early breast cancer progression events. During progression, as soon as microinvasive cell foci appear, recruitment of inflammatory cells is observed (data not shown). Tumor-bearing mice treated with Galunisertib reduced the proportion and tumor area of invasive foci. The proinflammatory role of TGF-β is well known during tumor progression[40] and although we cannot rule out that Galunisertib is acting by blocking the immune system, the tumor cells treated with the inhibitor present lower SMAD-4 positive cells compared to Controls. Thus, TGF-β signaling pathway is being blocked by the inhibitor in tumor cells. Similar to what we observed *in vitro*, SPARC and MT1-MMP expression is in consequence also reduced in Galunisertib treated tumours. All together, these findings lead us to propose that a mechanism that involves activated TGF-β pathway, induces sustained expression levels of SPARC and MT1-MMP, which are responsible for triggering pro-invasive mechanisms responsible for early transition in triple-negative breast cancer.

Lately, efforts have been made to develop specific tools that allow better understanding of the molecular signatures accompanying mechanisms that lead to the progression of carcinoma *in situ*[41]. In this work, we identify SPARC as an essential gene included in a molecular pathway involved during the DCIS-to-IDC transition, and we propose that the TGFBRI/SPARC/MT1-MMP axis may offer therapeutic targets to improve management of patients with *in situ* tumors.

Declaration Sections

Declarations

Ethics approval and consent to participate

This study complies with the Declaration of Helsinki, and was approved by each institution's internal review and ethics board (Comité de Pilotage du Groupe Sein, Institut Curie). Immunohistochemical (IHC) analysis of human samples was performed following approval by the institutional review board of the Comité de Ética en Investigación Clínica–Instituto Ángel H. Roffo (21/18).

Consent for publication

Not applicable

Availability of data and materials

All data will be available on request.

Competing interests

The authors declare no conflicts of interest.

Funding information

Agencia Nacional de Promocion Científica y Tecnologica (ANPCYT), Grant/Award Numbers: PICT 2018-03057, PICT 2016-0207; Fundación Fiorini, Grant/Award 2019; 2021 and UBACYT 20720190100005 BA; ICGex award by Institut Curie. Research Grant from HFSP (Human Frontier Science Program Grant No. RGP0032/2022 to P.J.S.), and the Deutsche Forschungsgemeinschaft (DFG, German Research Foundation)– Project-ID 335447717– SFB13228 (Project A20 to P.J.S.).

Author contribution

M.S. performed in vitro and vivo experiments, analysed the data and participated in the article conceptualization. M.P.C. contributed for the collection of the samples at the Institut, L.M. performed IHQ staing. M.P.C., C.L. and L.M. analysed clinical samples. E.L. and M.A performed the RNAseq analysis and analysed public transcriptome data set. N.P.C. assisted in vivo experiments. N.R.P, P.D.L, T.L.L. and K.P. performed in vitro experiments. AV-S selected and classified patients from PICBIM. E.R.B.

supervised patient's analysis. L.C and I.B. provided and analyzed clinical sample data. M.B., P.C., A.M.E. and P.S. assisted with resources, review and editing. C.L. supervised the project, designed experiments and wrote the manuscript.

Acknowledgements

The authors acknowledge the Breast Cancer Study Group and the Incentive and Cooperative Research Program "Breast cancer: Cell Invasion and Motility" of Institut Curie and all the staff of the Department of Pathology of the Diagnostic Area of the Angel Roffo Institute, specially Dr Fernando Carrizo, Fernanda Rocca and Gisela Lopez for their continued support. We also thank the patients from both institutions for the breast tumor samples. Dr Cecilia Perez Piñero and M. Sol Rodriguez for IHQ of PR and ER assistance. Authors also thank Dr Rebbeck for generously providing the timeline data documenting progression from normal breast tissue to invasive breast cancer. We also thank A. V. Failla and the UKE Microscopy Imaging Facility (UMIF) under the DFG Research Infrastructure Portal: RI–00489.

References

1. Bray F, Laversanne M, Sung H, Ferlay J, Siegel RL, Soerjomataram I, Jemal A. Global cancer statistics 2022: GLOBOCAN estimates of incidence and mortality worldwide for 36 cancers in 185 countries. CA Cancer J Clin. 2024;74(3):229–63. 10.3322/caac.21834.
2. C CF, W B, S RA, C.K.Y. N JH, K TA. J.S. RF. Progression from ductal carcinoma in situ to invasive breast cancer: Revisited. Mol Oncol. 2013;7(5):859–69. http://ovidsp.ovid.com/ovidweb.cgi?T=JS.&PAGE=reference&D=emed11&NEWS=N&AN=2013589080.
3. Lehman CD, Gatsonis C, Romanoff J, Khan SA, Carlos R, Solin LJ, Badve S, McCaskill-Stevens W, Corsetti RL, Rahbar H, Spell DW, Blankstein KB, Han LK, Sabol JL, Bumberry JR, Gareen I, Snyder BS, Wagner LI, Miller KD, Sparano JA, Comstock C. Association of Magnetic Resonance Imaging and a 12-Gene Expression Assay with Breast Ductal Carcinoma in Situ Treatment. JAMA Oncol. 2019;5(7):1036–42. 10.1001/jamaoncol.2018.6269.
4. Shaaban AM, Hilton B, Clements K, Provenzano E, Cheung S, Wallis MG, Sawyer E, Thomas JS, Hanby AM, Pinder SE, Thompson AM. Pathological features of 11,337 patients with primary ductal carcinoma in situ (DCIS) and subsequent events: results from the UK Sloane Project. Br J Cancer. 2021;124(5):1009–17. 10.1038/s41416-020-01152-5.
5. Punglia RS, Jiang W, Lipsitz SR, Hughes ME, Schnitt SJ, Hassett MJ, Nekhlyudov L, Achacoso N, Edge S, Javid SH, Niland JC, Theriault RL, Wong YN, Habel LA. Clinical risk score to predict likelihood of recurrence after ductal carcinoma in situ treated with breast-conserving surgery. Breast Cancer Res Treat. 2018;167(3):751–9. 10.1007/s10549-017-4553-5.
6. Nagasawa S, Kuze Y, Maeda I, Kojima Y, Motoyoshi A, Onishi T, Iwatani T, Yokoe T, Koike J, Chosokabe M, Kubota M, Seino H, Suzuki A, Seki M, Tsuchihara K, Inoue E, Tsugawa K, Ohta T, Suzuki Y. Genomic profiling reveals heterogeneous populations of ductal carcinoma in situ of the breast. Commun Biol. 2021;4(1):1–13. 10.1038/s42003-021-01959-9.

7. Allison KH, Hammond MEH, Dowsett M, McKernin SE, Carey LA, Fitzgibbons PL, Hayes DF, Lakhani SR, Chavez-MacGregor M, Perlmutter J, Perou CM, Regan MM, Rimm DL, Symmans WF, Torlakovic EE, Varella L, Viale G, Weisberg TF, McShane LM, Wolff AC. Estrogen and progesterone receptor testing in breast cancer: ASCO/CAP guideline update. J Clin Oncol. 2020;38(12):1346–66. 10.1200/JCO.19.02309.
8. Lodillinsky C, Infante E, Guichard A, Chaligné R, Fuhrmann L, Cyrta J, Irondelle M, Lagoutte E, Vacher S, Bonsang-Kitzis H, Glukhova M, Reyal F, Bièche I, Vincent-Salomon A, Chavrier P. p63/MT1-MMP axis is required for in situ to invasive transition in basal-like breast cancer. Oncogene. 2016;35(3):344–57. 10.1038/onc.2015.87.
9. Bumaschny V, Urtreger A, Diament M, Krasnapolski M, Fiszman G, Klein S. Joffé EB de K. Malignant myoepithelial cells are associated with the differentiated papillary structure and metastatic ability of a syngeneic murine mammary adenocarcinoma model. Breast Cancer Res. 2004;6(2). 10.1186/bcr757.
10. Martin C, Abba T, Gong Y, Lu J 2, Lee Y 2. Zhong2, Ezequiel Lacunza1, Matias Butti1, Yoko Takata2, Sally Gaddis2, Jianjun Shen2, Marcos R. Estecio2,3, Aysegul A. Sahin3 and CMA. A Molecular Portrait of High-Grade Ductal Carcinoma In Situ. *Cancer Res*. 2015;176(1):100–106.
11. Prat A, Cheang MCU, Martín M, Parker JS, Carrasco E, Caballero R, Tyldesley S, Gelmon K, Bernard PS, Nielsen TO, Perou CM. Prognostic significance of progesterone receptor-positive tumor cells within immunohistochemically defined luminal a breast cancer. J Clin Oncol. 2013;31(2):203–9. 10.1200/JCO.2012.43.4134.
12. Wolff AC, Hammond MEH, Hicks DG, Dowsett M, McShane LM, Allison KH, Allred DC, Bartlett JMS, Bilous M, Fitzgibbons P, Hanna W, Jenkins RB, Mangu PB, Paik S, Perez EA, Press MF, Spears PA, Vance GH, Viale G, Hayes DF. Recommendations for human epidermal growth factor receptor 2 testing in breast. J Clin Oncol. 2013;31(31):3997–4013. 10.1200/JCO.2013.50.9984.
13. Langle YV, Belgorosky D, Prack McCormick B, Sahores A, Góngora A, Baldi A, Lanari C, Lamb C, Eiján AM. FGFR3 Down-Regulation is Involved in bacillus Calmette-Guérin Induced Bladder Tumor Growth Inhibition. J Urol. 2016;195(1):188–97. 10.1016/j.juro.2015.06.093.
14. Bièche I, Parfait B, Tozlu SL, Lidereau R, Vidaud M. Quantitation of androgen receptor gene expression in sporadic breast tumors by real-time RT-PCR: Evidence that MYC is an AR-regulated gene. Carcinogenesis. 2001;22(9):1521–6. 10.1093/carcin/22.9.1521.
15. Sakurai-Yageta M, Recchi C, Le Dez G, Sibarita JB, Daviet L, Camonis J, D'Souza-Schorey C, Chavrier P. The interaction of IQGAP1 with the exocyst complex is required for tumor cell invasion downstream of Cdc42 and RhoA. J Cell Biol. 2008;181(6):985–98. 10.1083/jcb.200709076.
16. Saéz PJ, Vargas P, Shoji KF, Harcha PA, Lennon-Duméni AM, Saéz JC. ATP promotes the fast migration of dendritic cells through the activity of pannexin 1 channels and P2X7 receptors. Sci Signal. 2017;10(506):1–12. 10.1126/scisignal.aah7107.
17. Sáez PJ, Barbier L, Attia R, Thiam HR, Piel M, Vargas P. Leukocyte migration and deformation in collagen gels and microfabricated constrictions. Methods Mol Biol. 2018;1749:361–73.

10.1007/978-1-4939-7701-7_26.

18. Clausen BE, Amon L, Backer RA, Berod L, Bopp T, Brand A, Burgdorf S, Chen L, Da M, Distler U, Dress RJ, Dudziak D, Dutertre CA, Eich C, Gabele A, Geiger M, Ginhoux F, Giusiano L, Godoy GJ, Hamouda AEI, Hatscher L, Heger L, Heidkamp GF, Hernandez LC, Jacobi L, Kaszubowski T, Kong WT, Lehmann CHK, López-López T, Mahnke K, Nitsche D, Renkawitz J, Reza RA, Sáez PJ, Schlautmann L, Schmitt MT, Seichter A, Sielaff M, Sparwasser T, Stoitzner P, Tchitashvili G, Tenzer S, Tochoedo NR, Vurnek D, Zink F, Hieronymus T. Guidelines for mouse and human DC functional assays. Eur J Immunol. 2023;53(12):1–96. 10.1002/eji.202249925.
19. Behbod F, Kittrell FS, LaMarca H, Edwards D, Kerbawy S, Heestand JC, Young E, Mukhopadhyay P, Yeh HW, Allred DC, Hu M, Polyak K, Rosen JM, Medina D. An intraductal human-in-mouse transplantation model mimics the subtypes of ductal carcinoma in situ. Breast Cancer Res. 2009;11(5):1–11. 10.1186/bcr2358.
20. Teulière J, Faraldo MM, Shtutman M, Birchmeier W, Huelsken J, Thiery JP, Glukhova MA. β-Catenin-Dependent and -Independent Effects of ΔN-Plakoglobin on Epidermal Growth and Differentiation. Mol Cell Biol. 2004;24(19):8649–61. 10.1128/mcb.24.19.8649-8661.2004.
21. Cerami E, Gao J, Dogrusoz U, Gross BE, Onur S, Larsson E, Antipin Y, Reva B, Goldberg AP, Sander C. NIH Public Access. 2014;2(5):401–4. 10.1158/2159-8290.CD-12-0095.The.
22. Rebbeck CA, Xian J, Bornelöv S, Geradts J, Hobeika A, Geiger H, Alvarez JF, Rozhkova E, Nicholls A, Robine N, Lyerly HK, Hannon GJ. Gene expression signatures of individual ductal carcinoma in situ lesions identify processes and biomarkers associated with progression towards invasive ductal carcinoma. Nat Commun. 2022;13(1). 10.1038/s41467-022-30573-4.
23. Witkiewicz AK, Freydin B, Chervoneva I, Potoczek M, Rizzo W, Rui H, Brody JR, Schwartz GF, Lisanti MP. Stromal CD10 and SPARC expression in ductal carcinoma in situ (DCIS) patients predicts disease recurrence. Cancer Biol Ther. 2010;10(4):391–6. 10.4161/cbt.10.4.12449.
24. Lodillinsky C, Fuhrmann L, Irondelle M, Pylypenko O, Li XY, Bonsang-Kitzis H, Reyal F, Vacher S, Calmel C, De Wever O, Bièche I, Lacombe ML, Eiján AM, Houdusse A, Vincent-Salomon A, Weiss SJ, Chavrier P, Boissan M. Metastasis-suppressor NME1 controls the invasive switch of breast cancer by regulating MT1-MMP surface clearance. Oncogene. 2021;40(23):4019–32. 10.1038/s41388-021-01826-1.
25. Castro-Castro A, Marchesin V, Monteiro P, Lodillinsky C, Rossé C, Chavrier P. Cellular and Molecular Mechanisms of MT1-MMP-Dependent Cancer Cell Invasion. Annu Rev Cell Dev Biol. 2016;32:555–76. 10.1146/annurev-cellbio-111315-125227.
26. Said N. Role of SPARC in cancer; friend or foe. Ann Carcinog. 2016;1(1):1003.
27. Nagai MA, Gerhard R, Fregnani JHTG, Nonogaki S, Rierger RB, Netto MM, Soares FA. Prognostic value of NDRG1 and SPARC protein expression in breast cancer patients. Breast Cancer Res Treat. 2011;126(1):1–14. 10.1007/s10549-010-0867-2.
28. Zhu A, Yuan P, Du F, Hong R, Ding X, Shi X, Fan Y, Wang J, Luo Y, Ma F, Zhang P, Li Q, Xu B. SPARC overexpression in primary tumors correlates with disease recurrence and overall survival in patients

with triple-negative breast cancer. Oncotarget. 2016;7(47):76628–34. 10.18632/oncotarget.10532.

29. Guttlein LN, Benedetti LG, Fresno C, Spallanzani RG, Mansilla SF, Rotondaro C, Iraolagoitia XLR, Salvatierra E, Bravo AI, Fernandez EA, Gottifredi V, Zwirner NW, Llera AS, Podhajcer OL. Predictive outcomes for HER2-enriched cancer using growth and metastasis signatures driven by SPARC. Mol Cancer Res. 2017;15(3):304–16. 10.1158/1541-7786.MCR-16-0243-T.
30. Sangaletti S, Tripodo C, Santangelo A, Castioni N, Portararo P, Gulino A, Botti L, Parenza M, Cappetti B, Orlandi R, Tagliabue E, Chiodoni C, Colombo MP. Mesenchymal Transition of High-Grade Breast Carcinomas Depends on Extracellular Matrix Control of Myeloid Suppressor Cell Activity. Cell Rep. 2016;17(1):233–48. 10.1016/j.celrep.2016.08.075.
31. López-Moncada F, Torres MJ, Lavanderos B, Cerda O, Castellón EA, Contreras HR. SPARC Induces E-Cadherin Repression and Enhances Cell Migration through Integrin αvβ3 and the Transcription Factor ZEB1 in Prostate Cancer Cells. Int J Mol Sci. 2022;23(11). 10.3390/ijms23115874.
32. Hung JY, Yen MC, Jian SF, Wu CY, Chang WA, Liu KT, Hsu YL, Chong IW, Kuo PL. Secreted protein acidic and rich in cysteine (SPARC) induces cell migration and epithelial mesenchymal transition through WNK1/snail in non-small cell lung cancer. Oncotarget. 2017;8(38):63691–702. 10.18632/oncotarget.19475.
33. Tremble PM, Lane TF, Sage EH, Werb Z. SPARC, a secreted protein associated with morphogenesis and tissue remodeling, induces expression of metalloproteinases in fibroblasts through a novel extracellular matrix-dependent pathway. J Cell Biol. 1993;121(6):1433–44. 10.1083/jcb.121.6.1433.
34. McClung HM, Thomas SL, Osenkowski P, Toth M, Menon P, Raz A, Fridman R, Rempel SA. SPARC upregulates MT1-MMP expression, MMP-2 activation, and the secretion and cleavage of galectin-3 in U87MG glioma cells. Neurosci Lett. 2007;419(2):172–7. 10.1016/j.neulet.2007.04.037.
35. Gilles C, Bassuk JA, Pulyaeva H, Sage EH, Foidart JM, Thompson EW. SPARC/osteonectin induces matrix metalloproteinase 2 activation in human breast cancer cell lines. Cancer Res. 1998;58(23):5529–36.
36. Onorato M, Fiore A, Bayo E, Casali J, Fernandez-Tomé C, Rodríguez M, Domínguez M, Argemi L, Hidalgo J, Favre F, García C, Atorrasagasti M, Mazzolini C. SPARC inhibition accelerates NAFLD-associated hepatocellular carcinoma development by dysregulating hepatic lipid metabolism. Liver Int. 2021;41(7):1677–93. 10.1111/liv.14857.
37. Sun W, Feng J, Yi Q, Xu X, Chen Y, Tang L. SPARC acts as a mediator of TGF-β1 in promoting epithelial-to-mesenchymal transition in A549 and H1299 lung cancer cells. BioFactors. 2018;44(5):453–64. 10.1002/biof.1442.
38. Ham SM, Song MJ, Yoon HS, Lee DH, Chung JH, Lee ST. SPARC Is Highly Expressed in Young Skin and Promotes Extracellular Matrix Integrity in Fibroblasts via the TGF-β Signaling Pathway. Int J Mol Sci. 2023;24(15). 10.3390/ijms241512179.
39. Francki A, McClure TD, Brekken RA, Motamed K, Murri C, Wang T, Sage EH. SPARC regulates TGF-beta1-dependent signaling in primary glomerular mesangial cells. J Cell Biochem. 2004;91(5):915–25. 10.1002/jcb.20008.

40. Charles J, David JM. *Contextual Determinants of TGF-β Action in Development, Immunity and Cancer*.; 2018. 10.1038/s41580-018-0007-0.Contextual
41. Risom T, Glass DR, Averbukh I, Liu CC, Baranski A, Kagel A, McCaffrey EF, Greenwald NF, Rivero-Gutiérrez B, Strand SH, Varma S, Kong A, Keren L, Srivastava S, Zhu C, Khair Z, Veis DJ, Deschryver K, Vennam S, Maley C, Hwang ES, Marks JR, Bendall SC, Colditz GA, West RB, Angelo M. Transition to invasive breast cancer is associated with progressive changes in the structure and composition of tumor stroma. Cell. 2022;185(2):299–e31018. 10.1016/j.cell.2021.12.023.

Figures

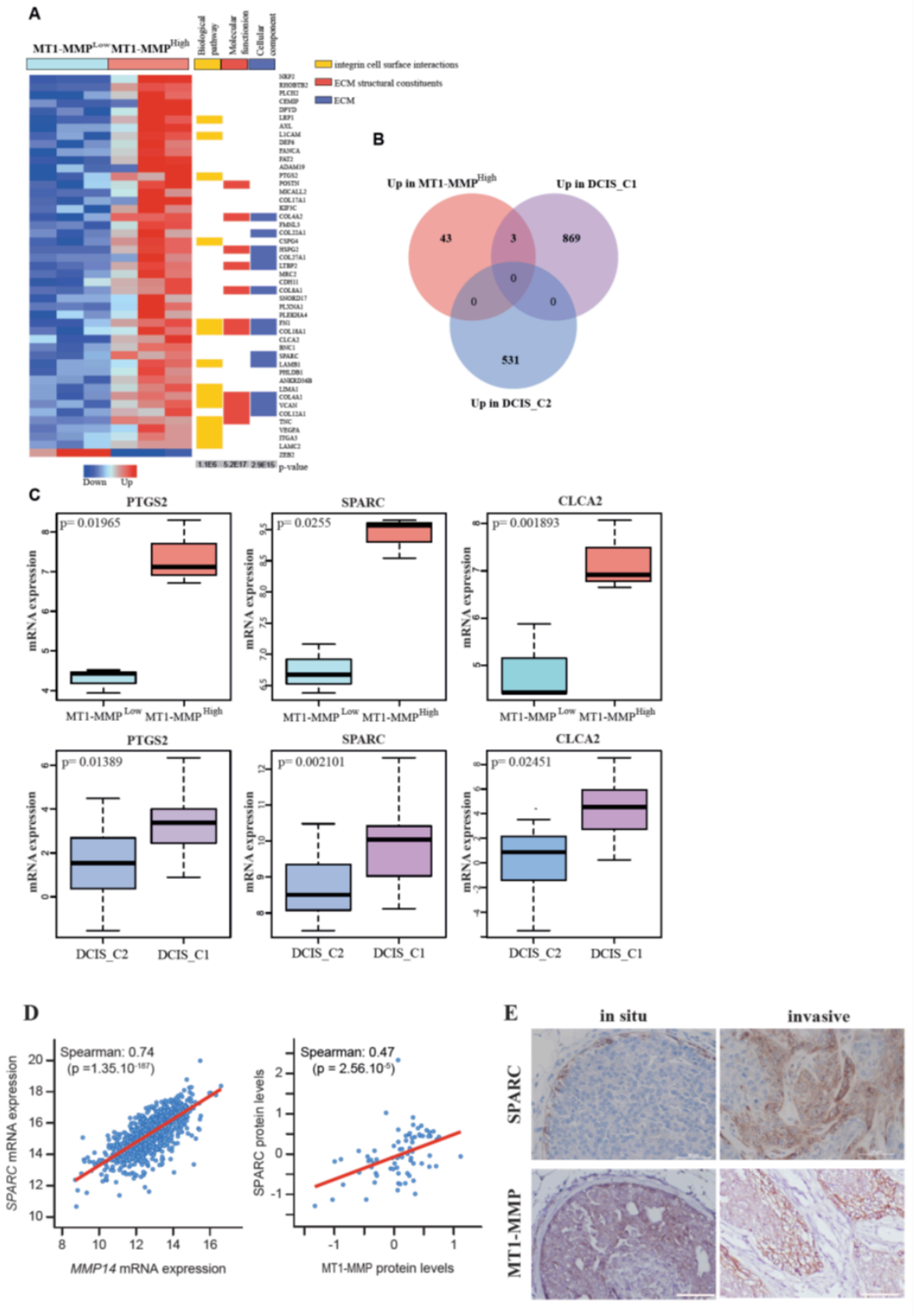
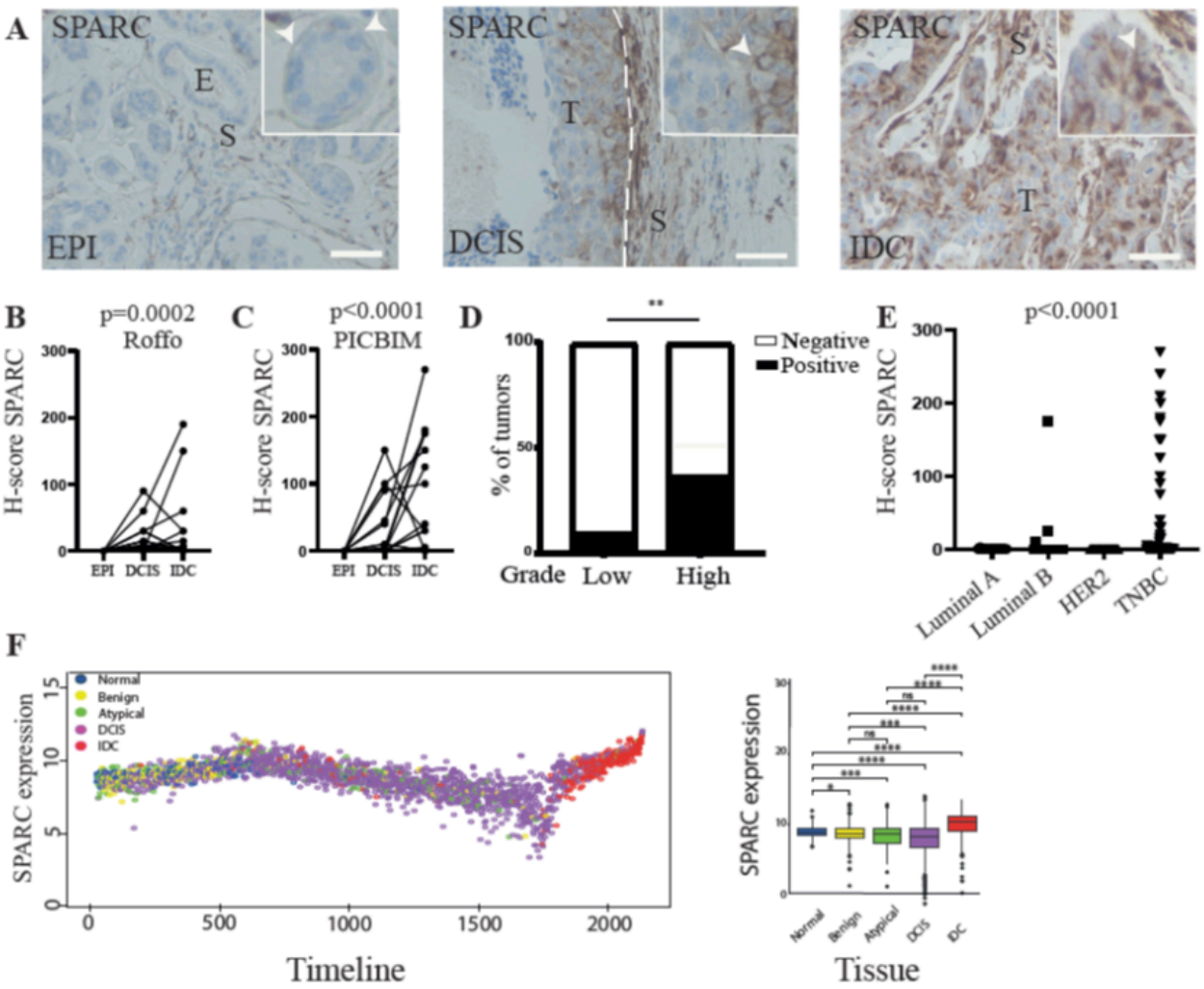


Figure 1

Screening of factors potentially involved in the early progression of breast cancer. A. Heat-map obtained after transcriptomic analysis of MT1-MMP^{high} versus MT1-MMP^{low} populations. **B**. Venn diagram of the list of differentially expressed genes between the DCIS-C1 and -C2 subgroups[10] with the genes upregulated in the MT1-MMP^{high} cell subpopulation. **C**. Box and whisker plots showing the

expression of genes in MT1-MMP^{high} and MT1-MMP^{low} in the MFC10DCIS.com cell population and in DCIS_C2 versus C1 groups. Upper panel PTGS2: p-value = 0.01965; SPARC: p-value = 0.0255; CLCA2: p-value = 0.001893 comparing MT1-MMP^{high} versus MT1-MMP^{low}. Lower panel: PTGS2: p-value **=** 0.01389; SPARC: p-value **=** 0.002101; CLCA2: p-value = 0.02451. **D**. **S**catter plot displaying the relationship between SPARC and MMP14 mRNA and protein levels in invasive breast carcinoma were retrieved from the TCGA database and analyzed for their correlation. The Spearman's rank correlation coefficients are indicated on each plot. SPARC and MMP14 correlated positively at both mRNA and protein levels. **E**. IHQ illustrating SPARC and MT1-MMP expression in in situ and invasive tumors after intraductal injection of MCF10DCIS. Scale bar: 50 µm.



DCIS	SPARC low	SPARC high
MT1-MMP low	21 (72 %)	1 (20 %)
MT1-MMP high	8 (28 %)	4 (80 %)

Figure 2

Overexpression of SPARC during human breast cancer progression. A. Representative SPARC IHC staining in breast peritumoral tissues and synchronous in situ and invasive components from one breast carcinoma biopsies. Dotted line separates stroma from de DCIS. E: Epithelium; T: Tumor; S: Stroma. Scale bar: 25µm. **B, C.** SPARC levels using the H-score method in the adjacent peritumoral tissues, in situ and invasive breast carcinomas in PICBIM's cohort (B)***p=0.0002, Friedman test and in Roffo's cohort

(C) ***p<0.001, Friedman test **D**. Proportion of cases regarding low (I and II) or high (III) histological grade **p=0.002 X^2 test, two-side. **E**. H-score of SPARC in IDC tumors of Roffo's cohort regarding molecular subtype, ***p<0.001 Kruskal-Wallis test. **F**. Left panel: Scatter plot illustrating the trend of SPARC expression -log2(CPM)-versus position along the timeline, during the progression from normal breast tissue to invasive breast cancer. Right panel: Box-plot illustrating SPARC expression into the different groups considered[22] *p<0.05; ***p<0.001; ****p<0.0001. ns non-significant Wilcoxon rank sum test **G**. Proportion of cases with high or low expression level of SPARC and MT1-MMP of consecutive slides. *p=0.0235 X^2 test, two-side. **H, I**. Representative IHQ staining in DCIS components for SPARC and MT1-MMP low (H) and high (I) expression levels. Scale bar: 50μm.

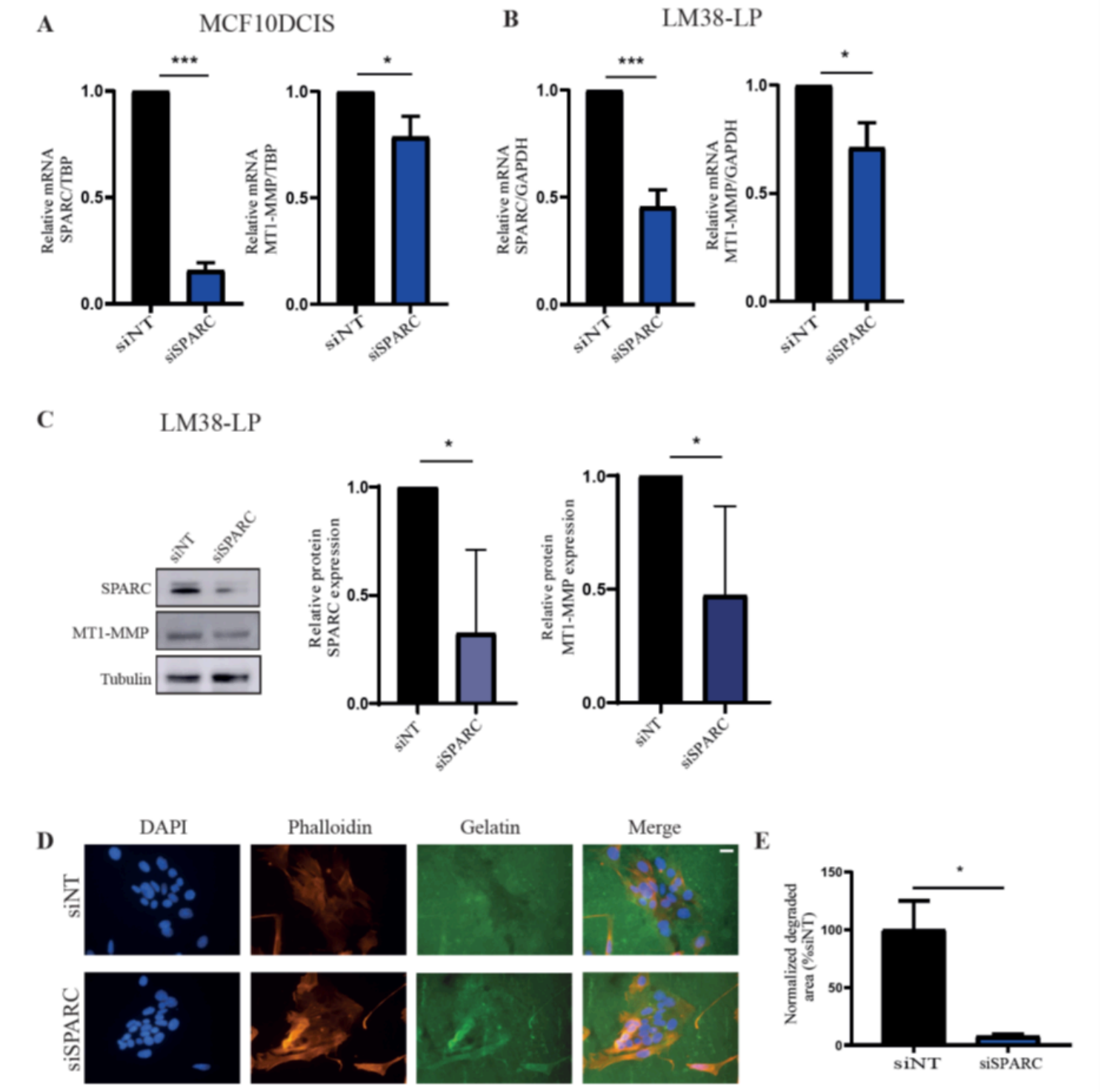


Figure 3

Pro-invasive role of SPARC mediated by MT1-MMP. A. SPARC and MT1-MMP expression at mRNA level in MCF10DCIS after transiently silenced for SPARC. Values corresponding to means ± SEM, n = 2 independent experiments of relative amounts of mRNA normalized against GAPDH and relativized to their CRL*** p<0.001, **p<0.01 t-test. **B.** SPARC and MT1-MMP expression at mRNA level in LM38-LP after transiently silenced for SPARC. Values corresponding to means ± SEM, n = 3 independent experiments of relative amounts of mRNA normalized against GAPDH and relativized to their CRL. ****

p<0.0001, *p<0.05 using one-side t-test. **C.** SPARC and MT1-MMP expression at protein level in LM38-LP after transiently silenced for SPARC (left). Values corresponding to means ± SEM, n = 3 independent experiments normalized against Tubulin and relativized to their CRL. *** p<0.001, *p<0.05 using one-side t-test. **D**. Representative images of cells in gelatin. Blue: DAPI, Green: Gelatin, Red: Phalloidin. Magnification bar: 50µm **E**. Quantification of fluorescent gelatin degradation by total cells in LM38-LP cells silenced or non-silenced for SPARC. Quantification of 1 assay (n=2). *p<0.05 using one-tailed t-test.

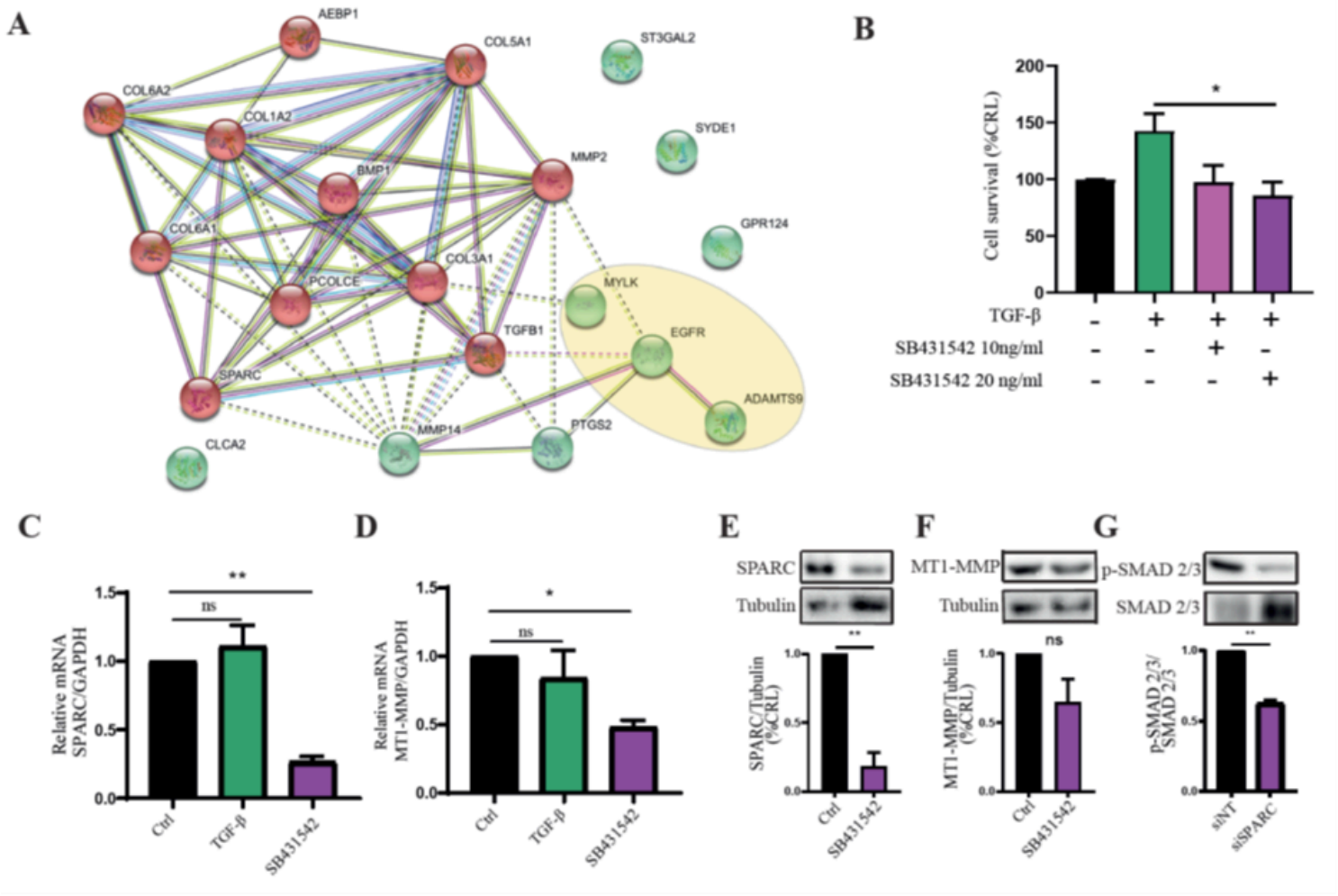


Figure 4

Rol of TGF-β molecular pathway in the SPARC pro-tumoral process. A. Association STRING analysis between the four candidate genes and co expressed genes. **B.** LM38-LP cells were treated with TGF-β (2ng/ml) and SB431542 (10 and 20 ng/ml) for 48 h, cell viability was evaluated by crystal violet assay. *p<0.05, **p< 0.01 by two-way ANOVA, Tukey's multiple comparisons test vs CRL. Values are means ± SEM, n=3 independent experiments. **C, D.**Expression mRNA level of SPARC (C) and MT1-MMP (D) in LM38-LP cells after SB431542 treatment (20ng/ml). Values corresponding to means ± SEM, n = 3 independent experiments of relative amounts of mRNA normalized against GAPDH and relativized to their CRL, t-test, *** p<0.0001. **E, F.** Protein levels of SPARC (E) and MT1-MMP (F) in LM38-LP cells after SB431542 treatment (20 ng/ml). Values corresponding to means ± SEM, n = 3. t-test, **p<0.001. **G.**

SMAD 2/3 phosphorylation was determined in LM38-LP cells transiently silenced for SPARC by Western Blot. Representative imaging and quantification. **p=0.0033 Unpaired t test, two-tailed, ns=non-significant.

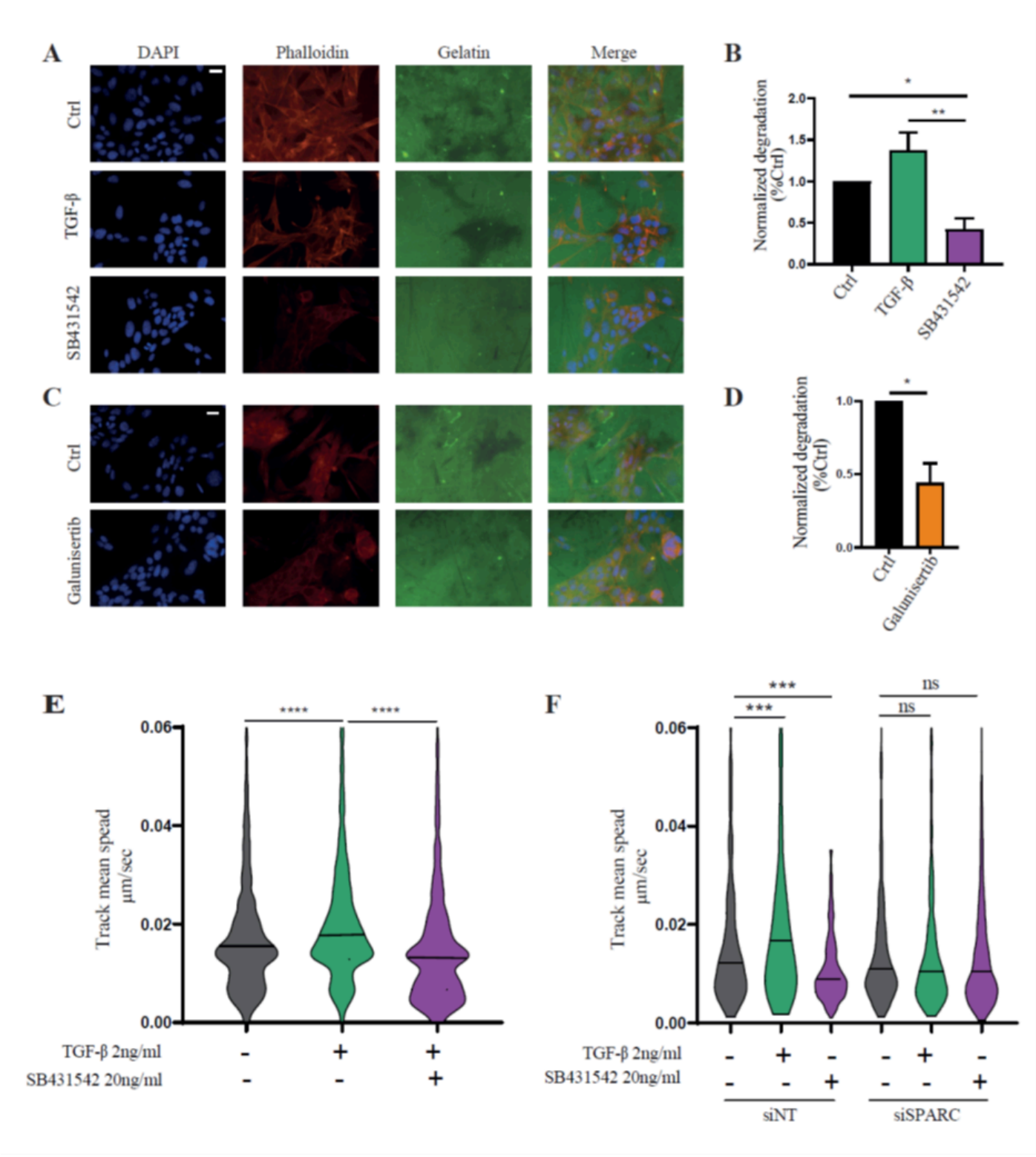


Figure 5

TGFBRI inhibition reduces matrix-degradative potential and motility of breast cancer cells. A. Representative images of the gelatin degradation assay of the murine LM38-LP cells treated or not with TGF-β(2 ng/ml) and SB431542 (20 ng/ml). Representative images of cells in fluorescent gelatin. Blue: DAPI, Green: Gelatin, Red: Phalloidin. Magnification bar: 50μm. **B**. Quantification of fluorescent gelatin degradation by total cells in LM38-LP cells, (n=4). *p<0,05, **p<0.001 using ANOVA-one way. **C.** Representative images of the gelatin degradation assay of the murine LM38-LP cells treated with Galunisertib (1 μg/ml). **D.**Quantification of fluorescent gelatin degradation by total cells in LM38-LP treated or not with Galunisertib (n=3). *p<0.05, using one tailed t-test. **E.** Single cell tracking assay in 3D collagen microdevise in LM38-LP cells treated or not with TGF-β and SB431542. Violin plot of track mean speed, *** p<0.0001, Kruskal-Wallis test. **F.** Single cell tracking assay in 2D in LM38-LP cells KO SPARC treated or not with TGF-β and SB431542. Violin plot of track mean speed, ***p<0.0001, Kruskal-Wallis test.

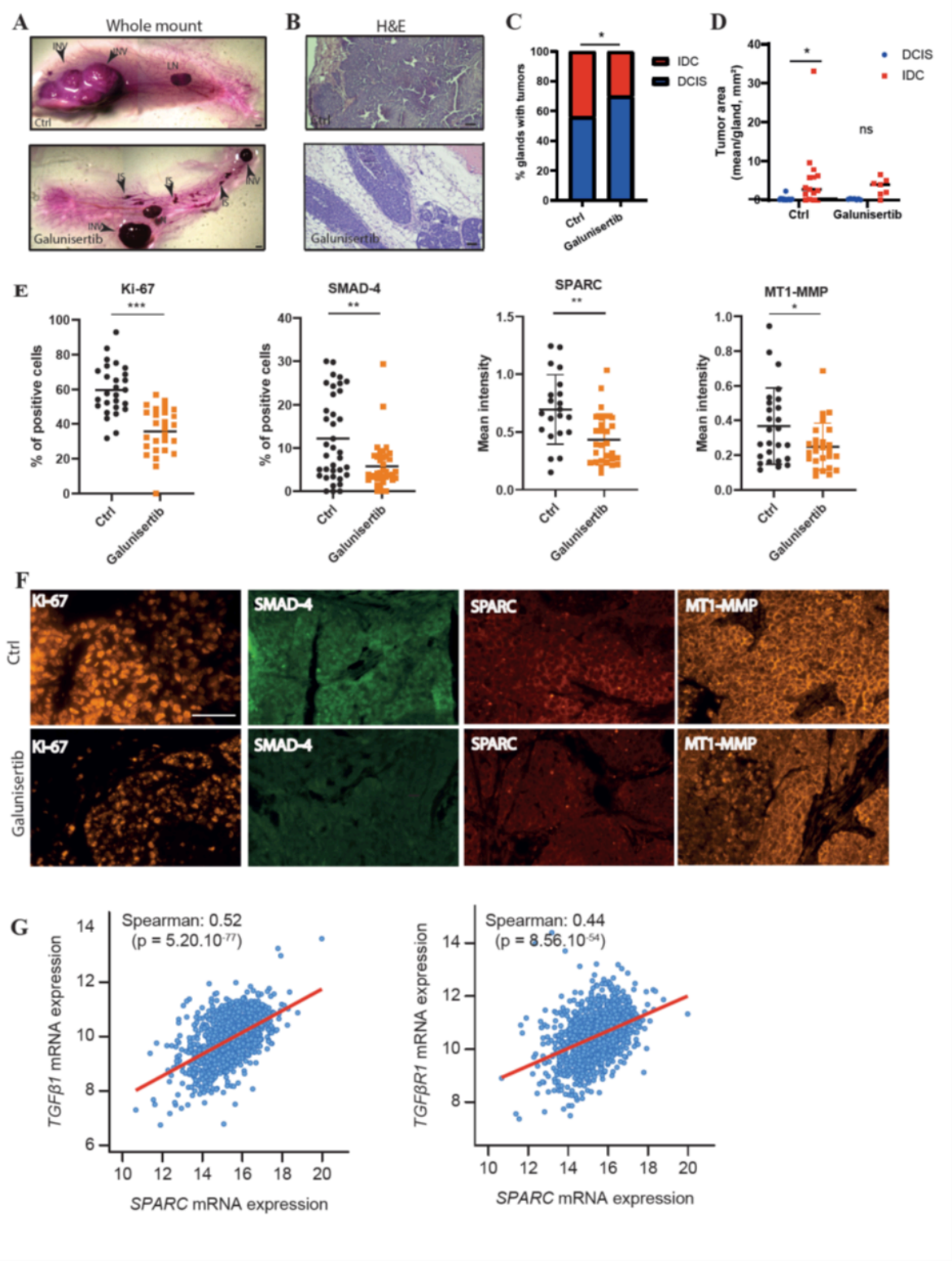


Figure 6

TGFBRI modulation impairs the *in situ* to invasive transition in the LM38-LP experimental model. A. Balb/c mice were intra-nipple injected with LM38-LP cells and treated or not with Galunisertib (60 mg/Kg). Representative images of the whole-mount carmine-stained glands analyzed 4-5 weeks after injection. IS, in situ; INV, invasive (Ctrl: n=15; Galunisertib n=18); LN, lymph node. Scale bar, 1 mm. **B.**Representative images of H&E tumors. Scale bar, 50 µm. **C.** Phenotypic analysis of intraductal

xenograft tumors of LM38-LP cells control or treated with Galunisertib. Analysis was based on whole-mount and H&E staining at 4–5 weeks after intraductal injection. Phenotypic analysis of intraductal xenograft tumors of LM38-LP cells treated or not with Galunisertib. The analysis was based on whole-mount Fisher's exact test, p= 0.0391. **D.** Tumor area per gland comparing progression status in Ctrl group and treated with Galunisertib. 2 ways ANOVA, Tukey's multiple comparisons test, p= 0.0418. **E-F** Percentage of positive cells for Ki-67, SMAD-4, SPARC and MT1-MMP markers by Immunofluorescence analyses in tissue sections in tumors treated or not with Galunisertib with the illustrative image. **p<0.01; *** p<0.001, Mann Whitney test, (pooled tumor from n=3 glands per group). Scale bar: 50 μm. **G**. **S**catter plot displaying the relationship between SPARC and TGF-β (left panel) and TGFBRI (right panel) mRNA levels in breast basal cancer tumors, based on data from the TCGA breast cancer dataset and analyzed for their correlation. The Spearman’s rank correlation coefficients are indicated on each plot. SPARC correlated positively with TGBI and TGFBRI at the mRNA level.

Supplementary Files

This is a list of supplementary files associated with this preprint. Click to download.

- Supptable1.pdf
- SupplementaryFileSiaccaetal.pdf
- CartaaprobacionCICUALLodillinsky022024.pdf
- SupplementalInformation.docx
- Supplfile1.xlsx